

Transport and diffusion of paramagnetic ellipsoidal particles in a rotating magnetic field

Jing-jing Liao^{1,2}, Wei-jing Zhu¹, and Bao-quan Ai^{1*}

¹ *Guangdong Provincial Key Laboratory of Quantum Engineering and Quantum Materials, School of Physics and Telecommunication Engineering, South China Normal University, Guangzhou 510006, China. and*

² *College of Applied Science, Jiangxi University of Science and Technology, Ganzhou 341000, China.*

(Dated: June 29, 2018)

Abstract

Transport and diffusion of paramagnetic ellipsoidal particles under the action of a rotating magnetic field are numerically investigated in a two-dimensional channel. It is found that paramagnetic ellipsoidal particles in a rotating magnetic field can be rectified in the upper-lower asymmetric channel. The transport and the effective diffusion coefficient are much more different and complicated for active particles, while they have similar behaviors and change a little when applying rotating magnetic fields of different frequencies for passive particles. For active particles, the back-and-forth rotational motion facilitates the effective diffusion coefficient and reduces the rectification, whereas the rotational motion synchronous with the magnetic field suppresses the effective diffusion coefficient and enhances the rectification. There exist optimized values of the parameters (the anisotropic degree, the amplitude and frequency of magnetic field, the self-propelled velocity, and the rotational diffusion rate) at which the average velocity and diffusion take their maximal values. Particles with different shapes, self-propelled speeds, or rotational diffusion rates will move to the opposite directions and can be separated by applying rotating magnetic fields of suitable strength and frequency. Our results can be used to separate particles, orient the particles along any direction at will during motion, and control the particle diffusion.

* Email: aibq@scnu.edu.cn

I. INTRODUCTION

Recently, transport and diffusion of Brownian particles in periodic structures have attracted considerable attention in biology, chemistry, and physics [1–11]. Different from passive colloids, self-propelled Brownian particles can produce a force which pushes them forward due to an internal mechanism which may be based on a light stimulus (thermophoresis) or concentration gradients (diffusophoresis) [12]. When colloidal particles are made using (or coated with) magnetic materials, they become responsive to external fields and show fascinating dynamical behavior which is of interest for both fundamental and technological aspects [13–25]. For example, circular motion of an active magnetic particle in a rotating magnetic field [14]; accumulating and clustering of magnetotactic bacteria under the effect of an external magnetic field [15, 16]; extracting work from magnetic-field-coupled Brownian particles [17]; fabrication and actuation of composites materials with magnetic torque [18]; manipulating and detecting biomaterials with magnetic torque [18] and other interesting transport and diffusion phenomena [19–25].

However, there exit few natural particles which have the perfect spherical symmetry. In contrast to isotropic particles, anisotropic magnetic colloids are characterized by an induced or spontaneous magnetization which has a dependence on a particular direction, feature the advantages of being easily torqued by an external field, and attract considerable interest in theoretical [26–30] and experimental studies [31–38]. Martin [26] studied a vortex magnetic field that can induce strong mixing in a magnetic particle suspension theoretically. Marino *et al.* [27] showed the rotational Brownian motion of colloidal particles in the over-damped limit generates an additional contribution to the "anomalous" entropy. Güell and coworkers [28] analyzed the diffusive properties of a paramagnetic passive particle torqued by a rotating magnetic field in the case of thermal noise considered. Fan and coworkers [29] studied the diffusion of an ellipsoidal self-driven particle under the effect of magnetic field, self-propulsion, and the particle's shape by finding approximated analytical expressions. Matsunaga and coworkers [30] showed how magnetic particles can be focused and segregated by size and shape by using a far-field hydrodynamic theory and simulations. Liu and their coworkers [31] experimentally showed separating superparamagnetic particles with a size difference around 130 nm by using periodically switching magnetic fields and asymmetric sawtooth channel sidewalls. Gao *et al.* [32]. demonstrated that magnetically

driven nanoswimmers provided a new approach for the rapid delivery of target-specific drug carriers to predetermined destinations. Hamilton *et al.* [33] demonstrated the experimental verification of a new class of autonomous ferromagnetic swimming devices, actuated and controlled solely by an oscillating magnetic field.

We are motivated by one of the previous experimental results describing the dynamics of paramagnetic ellipsoids in an external rotating magnetic field [37]. The researchers of the experiment found the ellipsoid mean rotation frequency and orientational angle of the elongated particles can be controlled by changing the frequency or strength of the applied field. They reported on subsequently a new technique for orienting self-driven microellipsoids by using an external field and the magnetic anisotropy of the ellipsoids [38]. In other studies related to the present work, how anisotropic magnetic particles under the action of an external field are rectified and diffuse in an asymmetric channel has not been considered yet, which results in peculiar behavior. In this paper, we consider paramagnetic ellipsoidal particles move in a two-dimensional asymmetric channel and are subject to an external magnetic field. We analyze transport and diffusion of paramagnetic ellipsoidal particles numerically. To focus on finding how the external magnetic field influences the transport and diffusion, we compare the transport and diffusion between the cases of active and passive particles. It is found that paramagnetic ellipsoidal particles in a rotating magnetic field can be rectified in the upper-lower asymmetric channel. The transport and the effective diffusion coefficient are much more different and complicated for active particles, while they have similar behaviors and change a little when applying rotating magnetic fields of different frequencies for passive particles. For active particles, there exist optimized values of the parameters (the anisotropic degree, the amplitude and frequency of magnetic field, the self-propelled velocity, and the rotational diffusion rate) at which the rectification and diffusion take their maximal values. Particles with different shapes, self-propelled speeds or rotational diffusion rates will move to the opposite directions and can be separated by applying rotating magnetic fields of suitable strength and frequency. Our results can be employed in several applications, such as particle separation, drug release and migration of contaminants in porous media.

II. MODEL AND METHODS

Inspired by finding transport and diffusion of paramagnetic ellipsoidal particles in the above experiment [37, 38], we consider noninteracting paramagnetic ellipsoidal particles of semimajor axis a and semiminor axis b , with preferred magnetization along semimajor axis. The particles move in a two-dimensional asymmetric channel and are subject to an external magnetic field of the form $\mathbf{H}(t) = H_0[\cos(\omega_H t), \sin(\omega_H t)]$ with angular frequency ω_H and amplitude H_0 (shown in Fig. 1). The particle at a given time t can be described by the position vector $\mathbf{R}(t)$ of its center of mass, which can be decomposed as $(\delta\hat{x}, \delta\hat{y})$ in the body frame and $(\delta x, \delta y)$ in the laboratory frame. $\theta(t)$ is the angle between the two frames. The swimming velocity (along its semimajor axis) of the self-propulsion particle is defined as the form $\mathbf{v} = v_0\mathbf{e}(t)$, where $\mathbf{e}(t) = [\cos\theta(t), \sin\theta(t)]$ is the instantaneous unit vector in the direction of swimming with its origin at the center of the particle, and v_0 is the magnitude of the swimming velocity. To focus on finding the effect of external magnetic fields, we choose dilute particles, hydrodynamic interactions and particle interactions will be negligible. Rotational and translational motion in the body frame are always decoupled, so the dynamics of the paramagnetic particle can be governed by the Langevin equations in a low-Reynolds-number environment and in the body frame [39–41],

$$\frac{d\hat{x}}{dt} = \Gamma_x[F_x \cos\theta(t) + F_y \sin\theta(t) + \hat{\xi}_x(t)] + v_0, \quad (1)$$

$$\frac{d\hat{y}}{dt} = \Gamma_y[F_y \cos\theta(t) - F_x \sin\theta(t) + \hat{\xi}_y(t)], \quad (2)$$

$$\frac{d\mathbf{e}(t)}{dt} = \boldsymbol{\Omega}(t) \times \mathbf{e}(t), \quad (3)$$

where Γ_x and Γ_y are the mobilities along its semimajor and semiminor axis, respectively. F_x and F_y are the forces along x and y direction of the laboratory frame. $\boldsymbol{\Omega}(t)$ is the swimmer's angular velocity. Equation (3) can be further simplified by a torque-balance condition on the ellipse:

$$\boldsymbol{\tau}_m + \boldsymbol{\tau}_H = \frac{\hat{\xi}_\theta(t)}{\Gamma_\theta}, \quad (4)$$

where Γ_θ is the rotational mobility, $\boldsymbol{\tau}_H = -\frac{\boldsymbol{\Omega}(t)}{\Gamma_\theta}$ represents the hydrodynamic torque, $\boldsymbol{\tau}_m = \mu_0\mathbf{m} \times \mathbf{H}$ is the magnetic torque (μ_0 is the magnetic susceptibility). The magnetic moment \mathbf{m} is defined as $\mathbf{m} = V\underline{\chi}\mathbf{H}$, where $V = \frac{4\pi}{3}ab^2$ and $\underline{\chi}$ is a second-order tensor representing the susceptibility of the ellipse. For the situation where there is a preferred magnetization

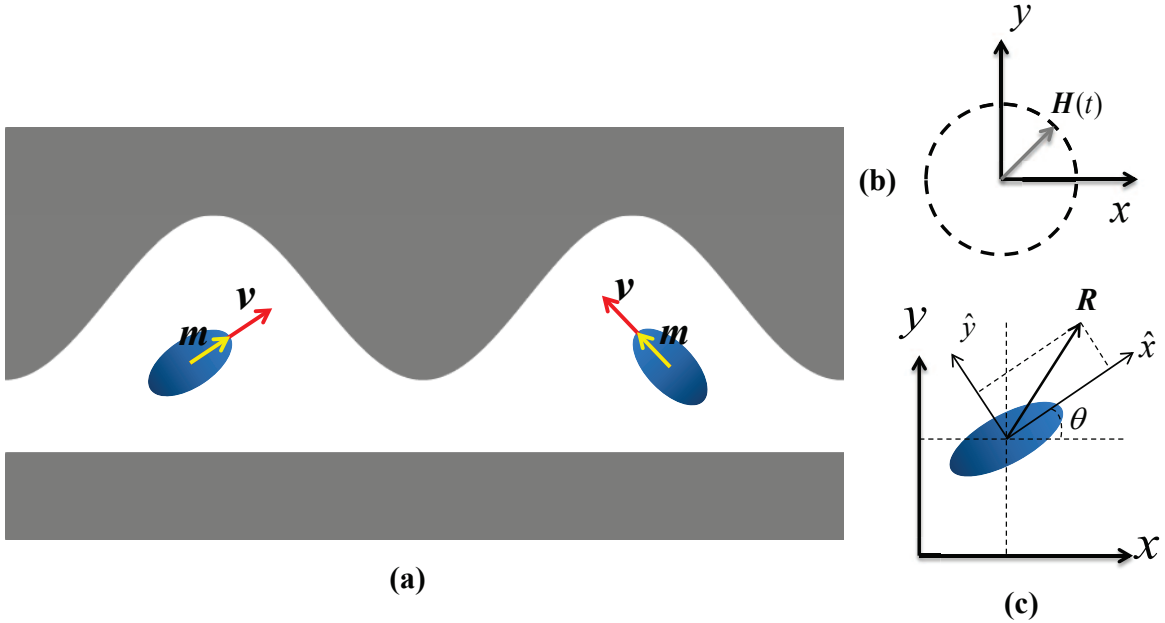


FIG. 1. Schematic of illustrating the system: (a) noninteracting paramagnetic Brownian swimmers with magnetic moment \mathbf{m} and swimming velocity \mathbf{v} moving in a two-dimensional asymmetric channel. (b) The swimmers are subject to a rotating magnetic field $\mathbf{H}(t) = H_0[\cos(\omega_H t), \sin(\omega_H t)]$. (c) Representation of an ellipsoid in the x - y laboratory frame and the \hat{x} - \hat{y} body frame. θ is the angle between two frames. \mathbf{R} is the position of the particle.

direction, the susceptibility tensor may be expressed as $\underline{\chi} = \chi_{\perp}\mathbf{I} + \Delta\chi\mathbf{e}\mathbf{e}$, where $\Delta\chi = \chi_{\parallel} - \chi_{\perp}$ and $\chi_{\parallel}(\chi_{\perp})$ is the susceptibility component parallel (normal) to \mathbf{e} . Equation (3) finally leads to

$$\frac{d\theta(t)}{dt} = \frac{\mu_0 V \Delta\chi H_0^2 \Gamma_\theta}{2} \sin[2(\omega_H t - \theta(t))] + \Gamma_\theta \hat{\xi}_\theta(t). \quad (5)$$

Note that the noise $\hat{\xi}_i(t)$ has mean zero and satisfies

$$\langle \hat{\xi}_i(t) \hat{\xi}_j(t') \rangle = \frac{2k_B T}{\Gamma_i} \delta_{i,j} \delta(t - t'), \quad i, j = x, y, \theta, \quad (6)$$

where T is the temperature and k_B is the Boltzmann constant.

We now obtain these equations in the laboratory frame. For convenience, converting the equation of motion to the fixed laboratory frame by using the rotation matrix:

$$R(\theta(t)) \equiv \begin{pmatrix} \cos \theta(t) & -\sin \theta(t) \\ \sin \theta(t) & \cos \theta(t) \end{pmatrix}, \quad (7)$$

The final set of equations describing the particle dynamics in the laboratory frame are:

$$\frac{dx}{dt} = v_0 \cos \theta(t) + F_x[\bar{\Gamma} + \Delta\Gamma \cos 2\theta(t)] + \Delta\Gamma F_y \sin 2\theta(t) + \xi_x(t), \quad (8)$$

$$\frac{dy}{dt} = v_0 \sin \theta(t) + F_y[\bar{\Gamma} - \Delta\Gamma \cos 2\theta(t)] + \Delta\Gamma F_x \sin 2\theta(t) + \xi_y(t), \quad (9)$$

$$\frac{d\theta(t)}{dt} = \omega_c \sin 2[\omega_H t - \theta(t)] + \xi_\theta(t), \quad (10)$$

where the critical frequency $\omega_c = \frac{\mu_0 V \Delta \chi H_0^2 \Gamma_\theta}{2}$, the quantities $\bar{\Gamma} = \frac{1}{2}(\Gamma_x + \Gamma_y)$ and $\Delta\Gamma = \frac{1}{2}(\Gamma_x - \Gamma_y)$ are the average and difference mobilities of the body, respectively. The parameter $\Delta\Gamma$ determines the asymmetry of the body, the particle is a perfect sphere for $\Delta\Gamma = 0$ and a very needlelike ellipsoid for $\Delta\Gamma \rightarrow \bar{\Gamma}$. $\xi_\theta(t)$ is a Gaussian random variable with zero mean and variance [41]:

$$\langle \xi_\theta(t) \xi_\theta(t') \rangle = 2D_\theta \delta(t - t'), \quad (11)$$

where $D_\theta = k_B T \Gamma_\theta$ is the rotational diffusion rate, which describes the nonequilibrium angular fluctuation. However, $\xi_x(t)$ and $\xi_y(t)$ are random Gaussian variables at fixed $\theta(t)$ with variance depending on the value of $\theta(t)$ [41],

$$\langle \xi_i(t) \xi_j(t') \rangle_{\theta(t)} = 2k_B T \Gamma_{ij} \delta(t - t'), \quad (12)$$

with $i, j = x, y$ and

$$\Gamma_{ij}[\theta(t)] = \bar{\Gamma} \delta_{ij} + \Delta\Gamma R[2\theta(t)] \cdot \begin{pmatrix} 1 & 0 \\ 0 & -1 \end{pmatrix}, \quad (13)$$

with Γ_{ij} the mobility tensor.

Usually, one of the critical elements of ratchet setup in nonlinear systems is asymmetry (temporal and/or spatial), which can violate the left-right symmetry of the response [42]. For our system, the asymmetry comes from the upper-lower asymmetry of the channel which is composed of the lower wall and the upper wall. Though the corrugated profile of the upper wall is left-right symmetric, the channel is upper-lower asymmetric. Coupling with the external field which induces the particles rotate, the upper-lower asymmetric channel can break the left-right symmetry and induce directed transport in the x direction. The lower wall of the channel is fixed as $w_l(x) = 0$, and the upper wall we choose corrugated structure [see Fig. 1(a)] can be described by

$$w_u(x) = c[\sin(\frac{2\pi x}{L})] + d, \quad (14)$$

where c and d are the parameters that control the shape of the upper wall. L is the periodicity of the channel. If we choose two simple walls, the channel is symmetric, and there is no directed transport.

In this paper, we use Brownian dynamic simulations performed by integration of the Langevin equations in the laboratory frame using the second-order stochastic Runge-Kutta algorithm. Because the particle along the y direction is confined, we only calculate the x direction average velocity based on Eqs. (8)-(10),

$$v_{\theta_0} = \lim_{t \rightarrow \infty} \frac{\langle x(t) \rangle_{\theta_0}^{\xi_x, \xi_y}}{t}, \quad (15)$$

where θ_0 is initial angle of the trajectory. The full average velocity after another average over all θ_0 is

$$v = \frac{1}{2\pi} \int_0^{2\pi} d\theta_0 v_{\theta_0}, \quad (16)$$

The scaled average velocity V_s is defined as $V_s = \frac{v}{v_0}$ for active particles, and the mobility μ is defined as $\mu = \frac{v}{f_0}$ for passive particles, where f_0 is the constant force applied at the particle along the x direction of the laboratory frame. And the effective diffusion coefficient along x direction is

$$D_x = \lim_{t \rightarrow \infty} \frac{\langle x^2(t) \rangle - \langle x(t) \rangle^2}{2t}, \quad (17)$$

. We use the scaled effective diffusion coefficient $D_{eff} = D_x/D_{free}$ for convenience, where $D_{free} = D_0 + v_0^2/2D_\theta$.

III. NUMERICAL RESULTS AND DISCUSSION

In our numerical simulations, the total integration time was more than 10^4 and the integration step time dt was chosen to be smaller than 10^{-3} . With these parameters, the simulation results are robust and do not depend on the time step and the integration time. Unless otherwise noted, we set $D_0 = 1.0$, $c = 0.6$, $d = L = 1.0$, $\bar{\Gamma} = 0.02$, $D_\theta = 0.1$, $v_0 = 3.5$ and $f_0 = 2.0$. Particle interactions are negligible. In the following discussion, we discuss the transport and diffusion for two cases: (A) rectification and diffusion of active particles ($v_0 \neq 0$, $f_0 = 0$) and (B) mobility and diffusion of passive particles ($v_0 = 0$, $f_0 \neq 0$).

A. Rectification and diffusion of active particles ($v_0 \neq 0, f_0 = 0$)

The dependence of the scaled average velocity V_s and the effective diffusion coefficient D_{eff} on the anisotropic parameter $\Delta\Gamma$ of active particles are presented in Fig. 2. When the particles are without a magnetic field ($\omega_c = 0$) or subject to a static magnetic field ($\omega_H = 0, \omega_c \neq 0$), shown in Fig. 2(a), V_s decreases monotonically with the increase of the anisotropic parameter $\Delta\Gamma$. The larger ω_c is, the bigger V_s is. When the particles are subject to a rotating magnetic field ($\omega_H \neq 0, \omega_c \neq 0$), V_s exhibits more complicated behavior. Figure 2(c) depicts the scaled average velocity V_s as a function of $\Delta\Gamma$ for different values of ω_c and ω_H at $v_0 = 2.0$. Figure 2(e) shows V_s as a function of $\Delta\Gamma$ for different values of v_0 at $\omega_c = 1.5$ and $\omega_H = 2.0$. We can find V_s increases as $\Delta\Gamma$ increases for some values while V_s is a peaked function of $\Delta\Gamma$ for other values. From Eq. (8), the self-propelled velocity v_0 , the critical frequency ω_c , the magnetic frequency ω_H and the anisotropic parameter $\Delta\Gamma$ compete with each other. When $0.75 \leq \omega_c/\omega_H \leq 1$ and $v_0 = 2.0, 3.5$, V_s is negative for suitable $\Delta\Gamma$. Therefore, for appropriate $\Delta\Gamma$, particles with different values of v_0 and subject to rotating magnetic fields of different frequencies and amplitudes move to different directions and can be separated. However, the effective diffusion coefficient D_{eff} decreases with increasing $\Delta\Gamma$ for $\omega_c/\omega_H > 1$ or $v_0 < 2.0$. And the effective diffusion coefficient is a peaked function of $\Delta\Gamma$ for the particles without a magnetic field, or subject to a static magnetic field, or a rotating magnetic field with $\omega_c/\omega_H \leq 1$ and $v_0 \geq 2.0$, shown in Figs. 2(b), 2(d), and 2(f).

Results for the scaled average velocity V_s and the effective diffusion coefficient D_{eff} as functions of the critical frequency ω_c for different magnetic frequencies ω_H are presented in Fig. 3. From Ref. [29], we know that the rotational deterministic dynamics of the ellipsoidal particle are different and depending on the ratio $\gamma \equiv \omega_c/\omega_H$. For the case $\gamma > 1$, the ellipsoidal particle rotates synchronously with the magnetic field. For the case $\gamma < 1$, the ellipsoidal swimmer performs a back-and-forth rotational motion which is considered as an asynchronous state due to the magnetic field, while it is trying to follow the rotation of the magnetic field. From Eq. (10), we can see that the self-propelled angle $\theta(t)$ is determined by the frequency ω_c , the magnetic frequency ω_H and the random noise. When the particles are subject to a static magnetic field ($\omega_H = 0$), shown in Fig. 3(a), no external field is applied to the particles for $\omega_c \rightarrow 0$; this means the ratchet disappears and the symmetry of the system cannot be broken, thus $V_s \rightarrow 0$. On increasing ω_c , the rotational motion synchronous with

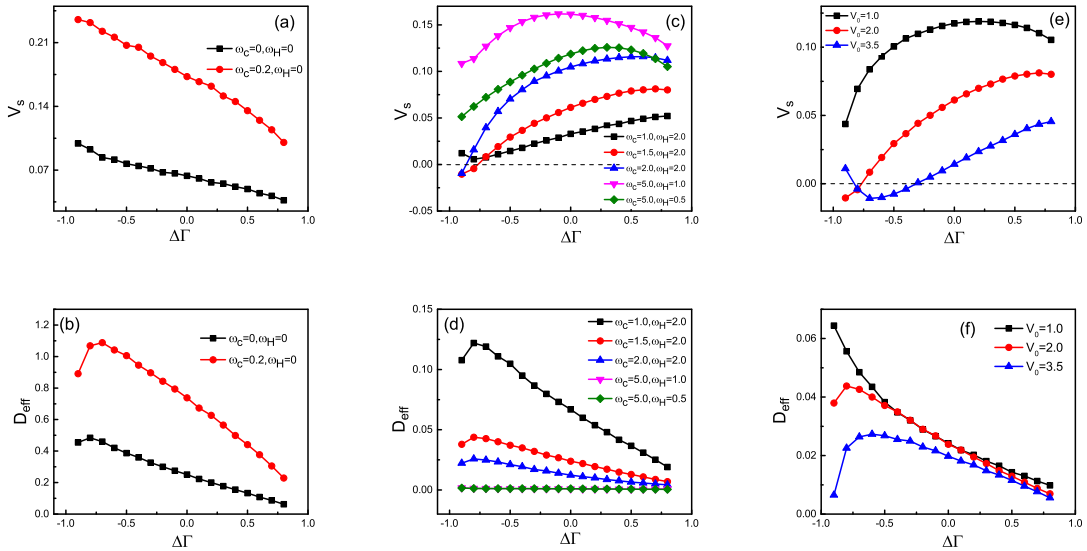


FIG. 2. Scaled average velocity V_s (a), (c) and the effective diffusion coefficient D_{eff} (b), (d) as functions of the anisotropic parameter $\Delta\Gamma$ of active particles for different values of ω_c and ω_H at $v_0 = 2.0$. Scaled average velocity V_s (e) and the effective diffusion coefficient D_{eff} (f) as functions of the anisotropic parameter $\Delta\Gamma$ of active particles for different values of v_0 at $\omega_c = 1.5$ and $\omega_H = 2.0$.

the magnetic field enhances the scaled average velocity V_s , thus V_s increases and reaches the maximal value. When the particles are subject to a rotating magnetic field ($\omega_H \neq 0$), shown in Fig. 3(c), both the magnetic frequency ω_H and frequency ω_c play the important roles and work together in the transport. When ω_c is small, i.e. $\gamma < 1$, the back-and-forth rotational motion reduces the mobility V_s , thus V_s reaches the minimum value which can be seen a valley in the curve. When ω_c increases to $\gamma > 1$, the rotational motion synchronous with the magnetic field enhances the mobility V_s , thus V_s reaches the maximal value which can be seen a peak in the curve. When $\omega_c \rightarrow \infty$, the self-propelled angle changes very fast and cannot feel the self-propelled driving, so $V_s \rightarrow 0$. It is noted that the position of the peak is the approximate value of ω_c at $\gamma \geq 1$ and shifts to large ω_c when ω_H increases.

From Fig. 3(b), it is found the giant acceleration of diffusion is observed at the critical ω_c . When ω_c is small, particles become trapped between potential barriers, and the external field dominates the diffusion. In this case, at the critical ω_c , particles can be driven out from the minima of the potential and can diffuse quickly through the potential, which leads to a large value of D_{eff} . When $\omega_c \rightarrow \infty$, particles rotate very fast, the influence of the external field

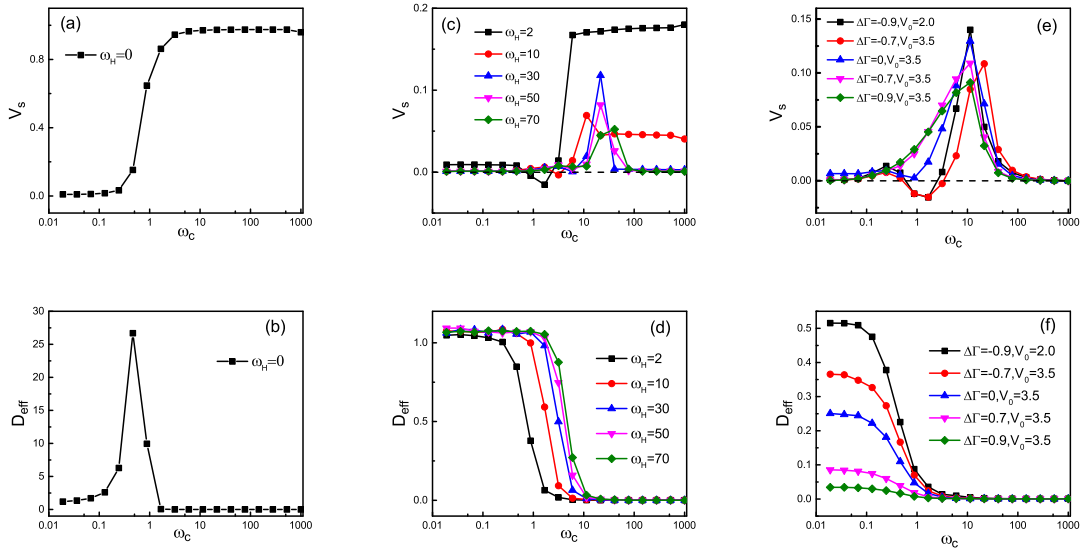


FIG. 3. Scaled average velocity V_s (a), (c) and the effective diffusion coefficient D_{eff} (b), (d) as functions of the critical frequency ω_c of active particles for different magnetic frequency ω_H at $\Delta\Gamma = -0.7$. Scaled average velocity V_s (e) and the effective diffusion coefficient D_{eff} (f) as functions of the critical frequency ω_c of active particles for different $\Delta\Gamma$ and v_0 at $\gamma = 0.75$.

can be neglected and particles are trapped in the valley of the potential, so $D_{eff} \rightarrow 0$. From Fig. 3(d), the effective diffusion coefficient D_{eff} decreases as the increase of ω_c . Namely, D_{eff} for $\gamma < 1$ is larger than that for $\gamma > 1$. In other words, the back-and-forth rotational motion facilitates the effective diffusion coefficient while the rotational motion synchronous with the magnetic field suppresses the effective diffusion coefficient. For different magnetic frequencies ω_H , the effective diffusion coefficients demonstrate similar behaviors and only exhibit a little difference for the position of the decreasing slope. It is noted that the scaled average velocity and effective diffusion coefficient are much larger when applying a static magnetic field ($\omega_H = 0$). Figure 3(e) and 3(f) address V_s and D_{eff} as functions of ω_c for different $\Delta\Gamma$ at $\gamma = 0.75$. We can find the variation of the maximal value of V_s and D_{eff} as the increasing $\Delta\Gamma$ is consistent with the results of Fig. 2(e) and 2(f). Remarkably, we note that current reversal occurs at $\Delta\Gamma = -0.9, -0.7$ by changing the magnetic frequency ω_c [shown in Figs. 3(c) and 3(e)].

Figure 4(a) describes the dependence of the scaled average velocity V_s on the magnetic frequency ω_H for different ω_c . Similar to the above results, the back-and-forth rotational motion facilitates the effective diffusion coefficient and reduces the rectification while the

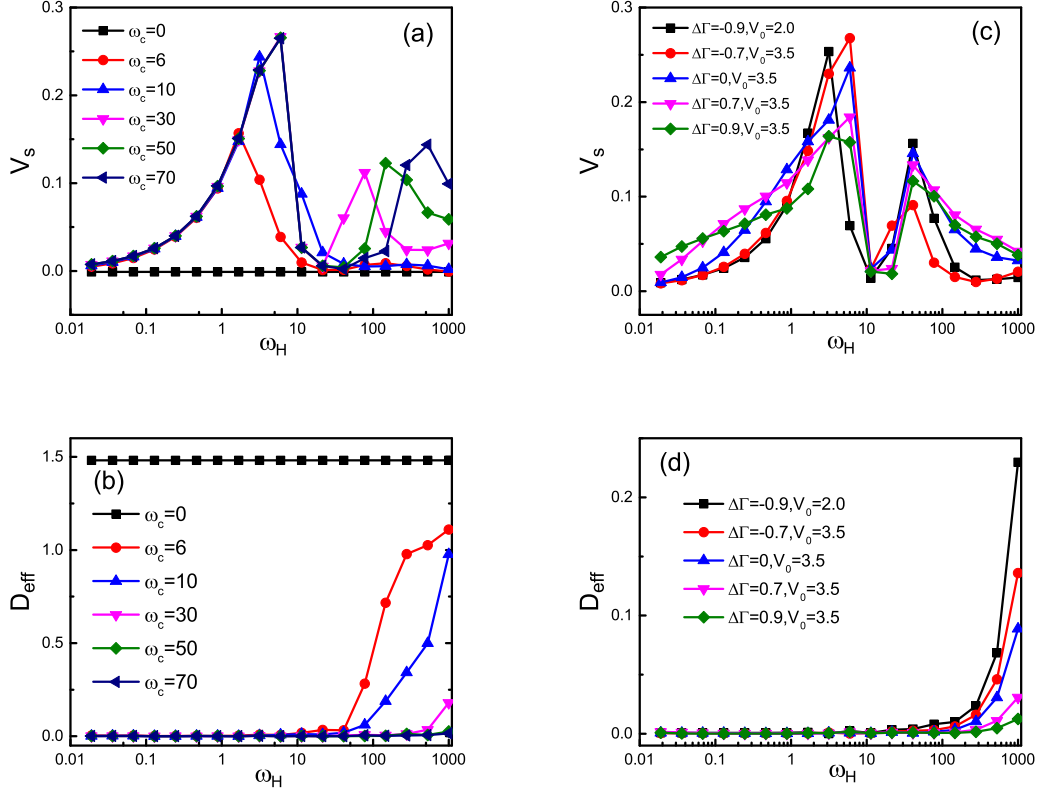


FIG. 4. Scaled average velocity V_s (a) and the effective diffusion coefficient D_{eff} (b) as functions of the magnetic frequency ω_H of active particles for different ω_c at $\Delta\Gamma = -0.7$. Scaled average velocity V_s (c) and the effective diffusion coefficient D_{eff} (d) as functions of the magnetic frequency ω_H of active particles for different $\Delta\Gamma$ and v_0 at $\omega_c = 20.0$.

rotational motion synchronous with the magnetic field reduces the effective diffusion coefficient and enhances the rectification. From Eqs. (8) and (10), we can see that the scaled average velocity V_s is determined by the self-propelled velocity v_0 , the self-propelled angle $\theta(t)$, the anisotropic parameter $\Delta\Gamma$ and the random noise, and the self-propelled angle $\theta(t)$ is a periodic function of ω_H . Thus, there exist two peak values of ω_H at which the scaled average velocity takes its maximal value. As ω_c increases, the peak value of V_s is bigger and the distance between two peak values is larger. From Fig. 4(b), it is found the effective diffusion coefficient D_{eff} increases as the increasing ω_H which indicates γ decreases. Namely, D_{eff} for $\gamma < 1$ is larger than that for $\gamma > 1$. For different frequencies ω_c , the

effective diffusion coefficients demonstrate similar behaviors and exhibit much difference for the position of the increasing slope. We note that the scaled average velocity is zero and the effective diffusion coefficient is constant when the particles are without magnetic field ($\omega_c = 0$). From Figs. 4(c) and 4(d), we can find the changing as the increasing $\Delta\Gamma$ of the maximal value of V_s and D_{eff} is consistent with the results of Figs. 2(e) and 2(f).

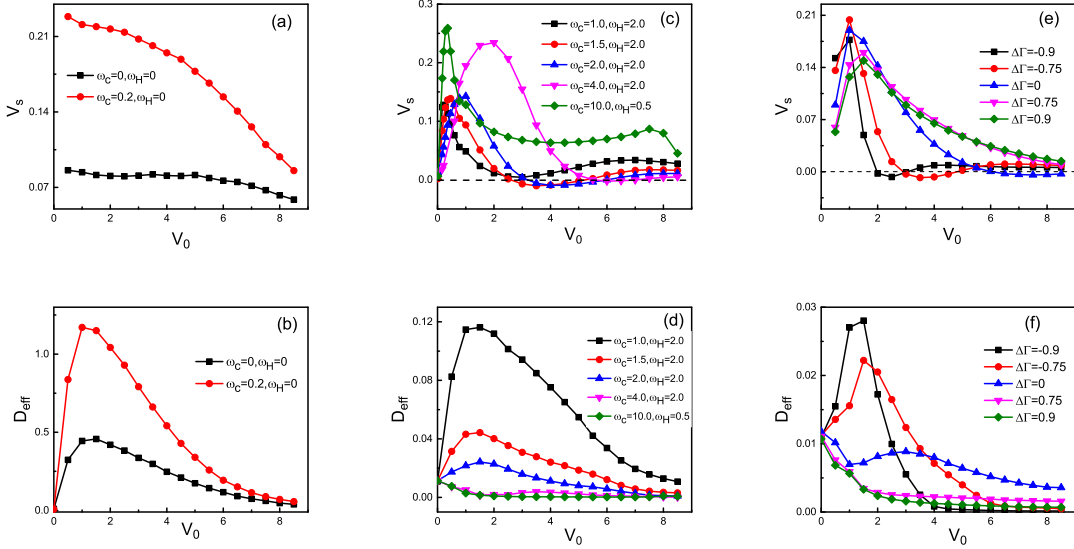


FIG. 5. Scaled average velocity V_s (a),(c) and the effective diffusion coefficient D_{eff} (b),(d) as functions of the self-propelled velocity v_0 of active particles for different values of ω_c and ω_H at $\Delta\Gamma = -0.6$. Scaled average velocity V_s (e) and the effective diffusion coefficient D_{eff} (f) as functions of the anisotropic parameter $\Delta\Gamma$ of active particles for different values of $\Delta\Gamma$ at $\omega_c = 1.5$ and $\omega_H = 2.0$.

Figure 5 displays the dependence of the scaled average velocity V_s and the effective diffusion coefficient D_{eff} on the self-propelled velocity v_0 . When the particles are without a magnetic field ($\omega_c = 0$) or subject to a static magnetic field ($\omega_H = 0, \omega_c \neq 0$), shown in Fig. 5(a), V_s decreases with increasing of v_0 . Figure 5(c) shows V_s as a function of v_0 for different ω_c and ω_H at $\Delta\Gamma = -0.6$. Figure 5(e) shows V_s as a function of v_0 for different $\Delta\Gamma$ at $\omega_c = 1.5$, $\omega_c = 2.0$. The term $v_0 \cos \theta(t)$ in Eq. (8) can be seen as the external driving force. When $v_0 \rightarrow 0$, the external driving force can be negligible, so $V_s \rightarrow 0$. For very large values of v_0 , the influence of external field can be negligible, so V_s decreases. Therefore, there exists an optimal value of v_0 at which V_s takes its maximal. Remarkably, V_s is negative for suitable v_0 when $0.75 \leq \omega_c/\omega_H \leq 1$ and $\Delta\Gamma = -0.6, -0.75, -0.9$. Therefore,

the rectified direction of particles with different shapes and subject to magnetic fields of different frequencies and amplitudes can be reversed by changing v_0 . From Figs. 5(b), 5(d) and 5(f), we can find the effective diffusion coefficient D_{eff} decreases monotonically with increasing of v_0 when $\Delta\Gamma > 0$, while D_{eff} is a peak function of v_0 when $\Delta\Gamma \leq 0$. The nonmonotonic behaviors observed in Fig.5 share similarities with negative differential and absolute mobility effects observed in different systems, such as the driven lattice gas models [43–46], driven particles adverted by laminar flows [47, 48], and active matter [49].

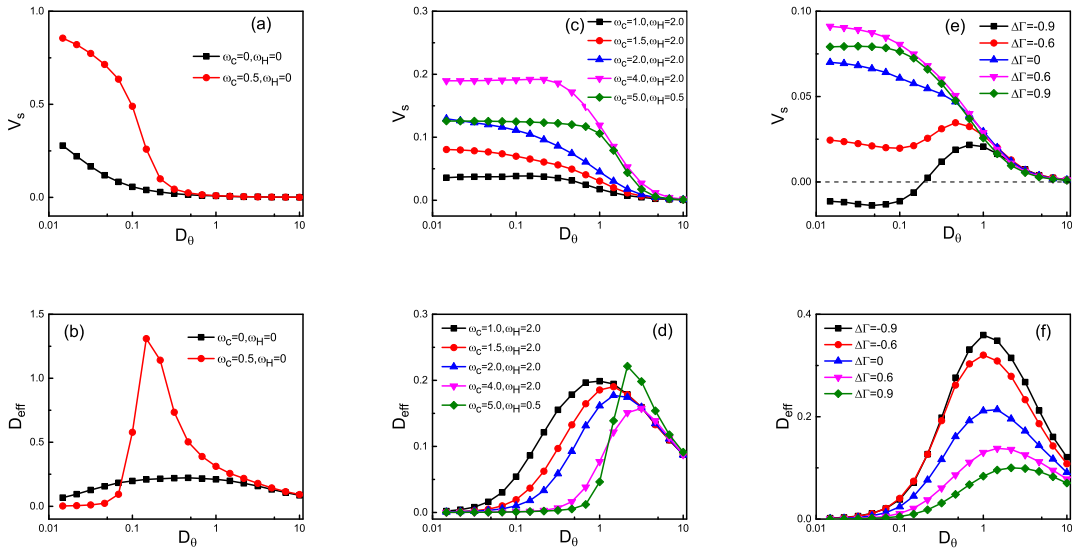


FIG. 6. Scaled average velocity V_s (a),(c) and the effective diffusion coefficient D_{eff} (b),(d) as functions of the rotational diffusion D_θ of active particles for different values of ω_c and ω_H at $\Delta\Gamma = 0.2$ and $v_0 = 2.0$. Scaled average velocity V_s (e) and the effective diffusion coefficient D_{eff} (f) as functions of the anisotropic parameter $\Delta\Gamma$ of active particles for different values of $\Delta\Gamma$ at $\omega_c = 1.5$, $\omega_H = 2.0$, and $v_0 = 2.0$.

The scaled average velocity V_s and the effective diffusion coefficient D_{eff} as functions of the rotational diffusion D_θ are shown in Fig. 6. From Fig. 6(a), we can find when the particles are without a magnetic field ($\omega_c = 0$), V_s decreases slowly with the increase of D_θ . When applying a static magnetic field ($\omega_H = 0$, $\omega_c \neq 0$), the curve is convex. This phenomenon can be easily explained by introducing the two factors: (A) the increase of ω_c enhances the rectification and (B) the increase of D_θ reduces the rectification. For the case without an external field, factor B dominates the transport. When $D_\theta \rightarrow 0$, the self-propelled angle θ almost does not change, and V_s approaches its maximal value. When

$D_\theta \rightarrow \infty$, the particles cannot feel the self-propelled driving and are trapped in the valley of the potential, so $V_s \rightarrow 0$. For the case of applying a static magnetic field, factor A determines the transport, V_s reduces slowly, and finally factor B also becomes important, V_s reduces quickly, so the curve is convex. Besides, the bigger ω_c is, the larger the maximal value V_s approaches. Figure 6(c) shows V_s decreases monotonically as D_θ increases and finally tends to be zero when applying a rotating magnetic field. It is also found that the maximal value V_s is the biggest when $\omega_c = 4.0$, $\omega_H = 2.0$. As the above results, the ellipse rotates synchronously with the magnetic field for $\gamma > 1$, but performs a back-and-forth rotational motion for $\gamma < 1$. In other words, the rotational motion synchronous with the magnetic field facilitates the rectification while the back-and forth rotational motion reduces the rectification. The nearer to $\gamma = 1$, the larger the maximal value V_s is. Figure 6(e) presents V_s as a function of the rotational diffusion D_θ for different values of $\Delta\Gamma$ at $\omega_c = 1.5$, $\omega_H = 2.0$. V_s decreases monotonically as D_θ increases for $\Delta\Gamma \geq 0$ while there exists an optimal value of D_θ at which V_s takes its maximal value for $\Delta\Gamma < 0$. Because $\Delta\Gamma$ can reduce the growth of V_s when $\Delta\Gamma < 0$ which have been found from Fig. 2. Remarkably, the rectified direction can be reversed by changing D_θ when $\Delta\Gamma = -0.9$. Therefore, for suitable D_θ , particles with different shapes will move to the opposite directions and can be separated.

The effective diffusion coefficient D_{eff} as a function of D_θ exhibits a pronounced resonance peak in the curve [shown in Fig. 6(b), 6(d), and 6(f)]. This is due to the mutual interplay between the external field and the rotational diffusion rate. When D_θ is small, the external field dominates the diffusion. When $D_\theta \rightarrow \infty$, particles rotate very fast, the influence of the external field can be neglected and particles are trapped in the valley of the potential, so $D_{eff} \rightarrow 0$. Especially, when applying a static field, particles can be driven out from the minima of the potential and can diffuse quickly through the potential, which leads to a large value of D_{eff} . Therefore, D_{eff} is much larger than 1, shown in Fig. 6(b) for $\omega_H = 0$, $\omega_c \neq 0$, which indicates the giant acceleration of diffusion. In addition, from Fig. 6(d), the amplitude of the peak decreases and the position of the peak shifts to large D_θ when ω_c/ω_H increases. From Fig. 6(f), the maximal value of D_{eff} decreases with increasing $\Delta\Gamma$ which is accordance to Fig. 2.

B. Mobility and diffusion of passive particles ($v_0 = 0, f_0 \neq 0$)

The results for the mobility μ and the effective diffusion coefficient D_{eff} depending on the anisotropic parameter $\Delta\Gamma$ of passive particles are presented in Fig. 7. We can find the mobility and the effective diffusion coefficient have similar behaviors. When the particles are subject to a static magnetic field ($\omega_H = 0, \omega_c \neq 0$), μ and D_{eff} increase with increasing $\Delta\Gamma$. While there exists an optimal value of $\Delta\Gamma$ where μ and D_{eff} are maximal when the particles are without an external field or subject to a rotating magnetic field. μ and D_{eff} of anisotropic particles are smaller than that of isotropic particles. Additionally, the mobility μ and the effective diffusion coefficient D_{eff} change a little when applying rotating magnetic fields of different frequencies.

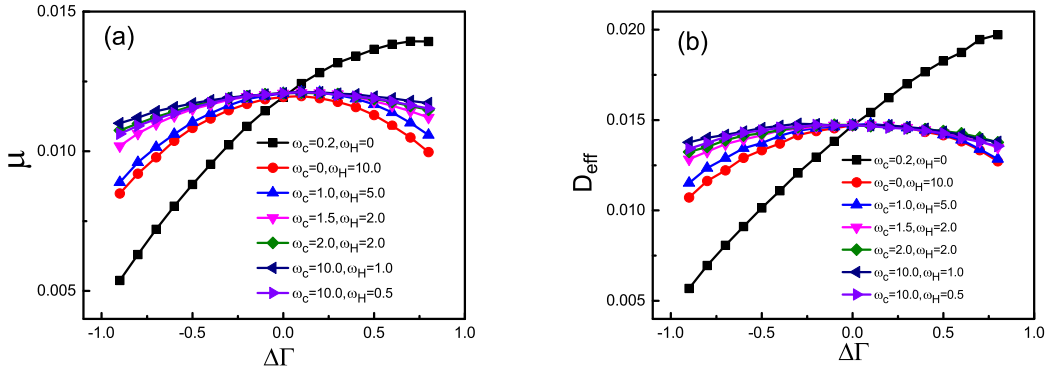


FIG. 7. The mobility μ (a) and the effective diffusion coefficient D_{eff} (b) as functions of the anisotropic parameter $\Delta\Gamma$ of passive particles for different values of ω_c and ω_H .

In Fig. 8, we plot the mobility μ and the effective diffusion coefficient D_{eff} as functions of the critical frequency ω_c of passive particles. It is found the mobility and the effective diffusion coefficient have also similar behaviors and increase as the increasing ω_c and then remain constant values. Namely, the frequency ω_c facilitates the mobility and the effective diffusion coefficient first, and plays little influence finally. As we know, for the case $\gamma > 1$, the ellipsoidal particle rotates synchronously with the magnetic field. For the case $\gamma < 1$, the ellipsoidal swimmer performs a back-and-forth rotational motion which is considered as an asynchronous state. Especially, μ and D_{eff} of the particles which are subject to a static

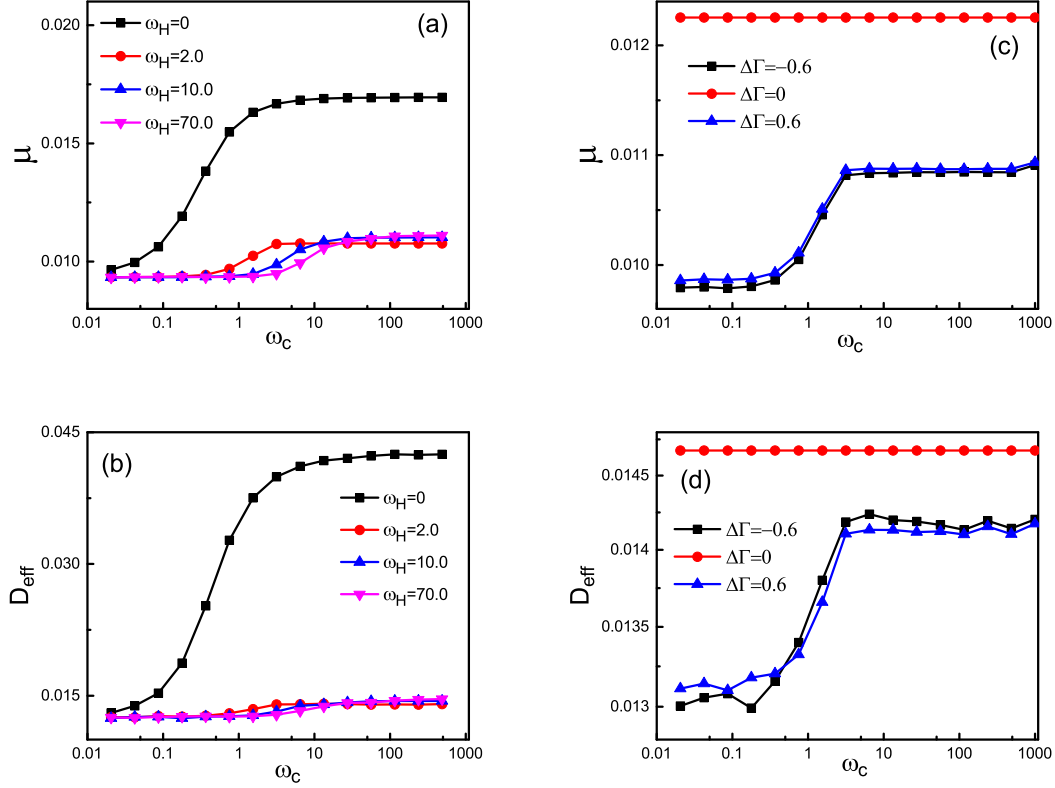


FIG. 8. The mobility μ (a) and the effective diffusion coefficient D_{eff} (b) as functions of the critical frequency ω_c of passive particles for different magnetic frequency ω_H at $\Delta\Gamma = 0.7$. The mobility μ (c) and the effective diffusion coefficient D_{eff} (d) as functions of the critical frequency ω_c of passive particles for different $\Delta\Gamma$ at $\omega_H = 2.0$.

field ($\omega_H = 0$) are much larger than that of the particles which are subject to a rotating field ($\omega_H \neq 0$) from Figs. 8(a) and 8(b). In the other hand, μ and D_{eff} only exhibit a little difference when changing the value of ω_H . The position of reaching the maximum is the approximate value of ω_c at $\gamma \geq 1$ and shifts to large ω_c when ω_H increases. From Figs. 8(c) and 8(d), we can find μ and D_{eff} remain constant values for isotropic particles ($\Delta\Gamma = 0$), and are always larger than that of anisotropic particles which can be also demonstrated in Fig. 7.

From Fig. 9, we can find the mobility μ and the effective diffusion coefficient D_{eff} depend on the magnetic frequency ω_H of passive particles. When the particles are without

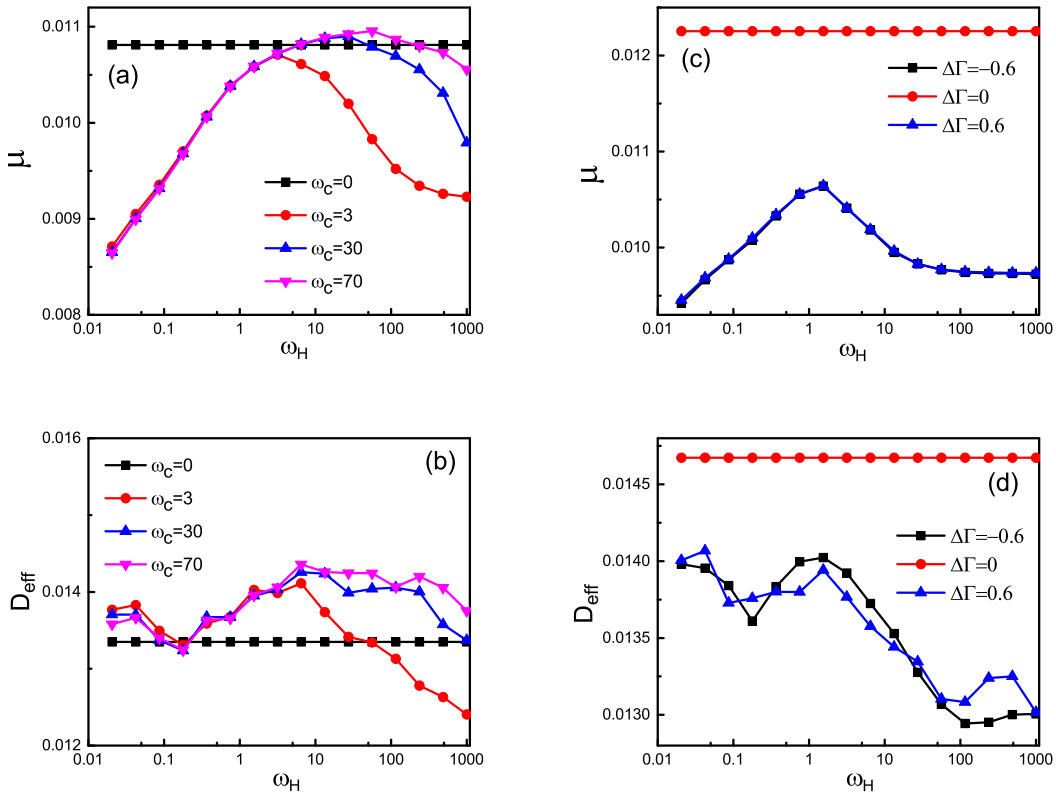


FIG. 9. The mobility μ (a) and the effective diffusion coefficient D_{eff} (b) as functions of the magnetic frequency ω_H of passive particles for different ω_c at $\Delta\Gamma = 0.7$. The mobility μ (c) and the effective diffusion coefficient D_{eff} (d) as functions of the magnetic frequency ω_H of passive particles for different $\Delta\Gamma$ at $\omega_c = 2.0$.

an external field ($\omega_c = 0$), μ and D_{eff} remain unchanged. When the particles are subject to a rotating field, the rotational motion synchronous with the magnetic field for $\gamma > 1$ enhances the mobility first, then the back-and-forth rotational motion for $\gamma < 1$ reduces the mobility. Thus, there exists one optimal value of ω_H at which the mobility takes its maximal value. The position of the peak is nearly to $\omega_H \leq \omega_c$. However, the effective diffusion coefficient decreases first, then increases, and finally decreases to a constant value, shown in Fig. 9(b). There exist two peak values of ω_H . From Figs. 9(c) and 9(d), we can also find μ and D_{eff} remain constant values for isotropic particles ($\Delta\Gamma = 0$), and are always larger than that of anisotropic particles which are similar to the above results.

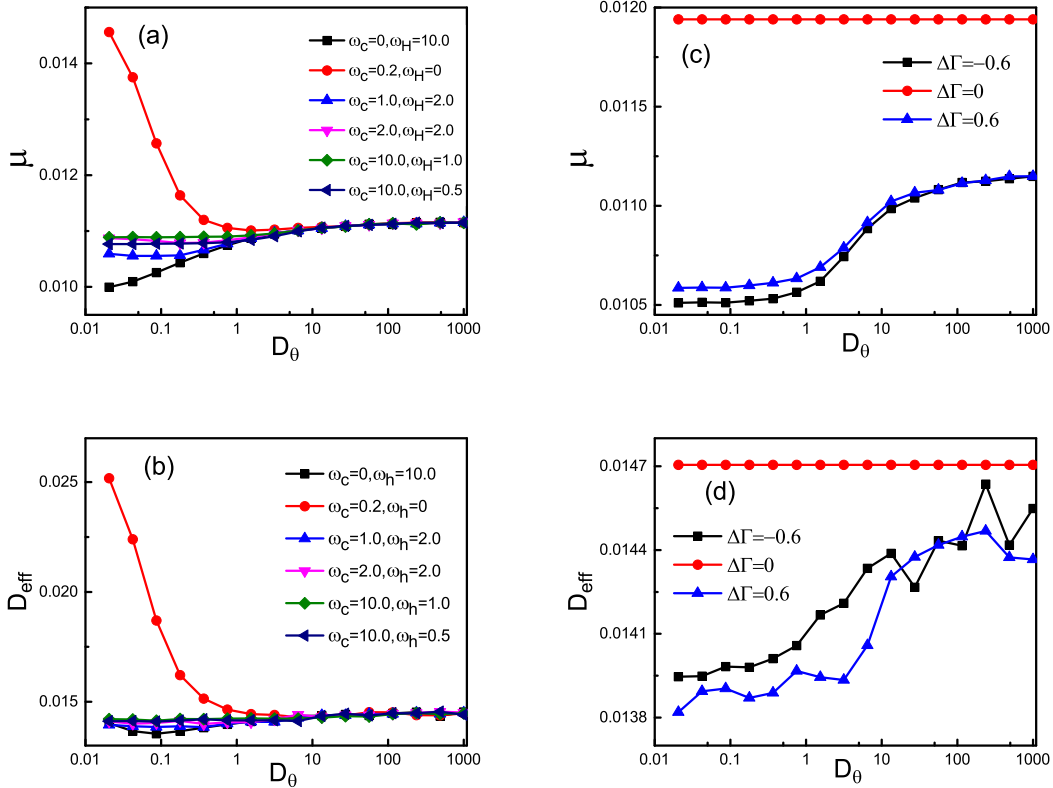


FIG. 10. The mobility μ (a) and the effective diffusion coefficient D_{eff} (b) as functions of the rotational diffusion D_θ of passive particles for different values of ω_c and ω_H at $\Delta\Gamma = 0.5$. The mobility μ (c) and the effective diffusion coefficient D_{eff} (d) as functions of the rotational diffusion D_θ of passive particles for different values of $\Delta\Gamma$ at $\omega_c = 10.0$ and $\omega_H = 0.5$.

Figure 10 addresses the mobility μ and the effective diffusion coefficient D_{eff} as functions of the rotational diffusion D_θ of passive particles. From Figs. 10(a) and 10(b), the behaviors of the mobility μ and the effective diffusion coefficient D_{eff} for the case of a static magnetic field ($\omega_H = 0$, $\omega_c \neq 0$) are different from that for other cases. When the particles are subject to a static magnetic field, μ and D_{eff} decrease with the increase of D_θ . Because the rotational motion synchronous with the magnetic field enhances the mobility and the effective diffusion coefficient. When $D_\theta \rightarrow 0$, the external field plays a key role in the mobility and the effective diffusion coefficient, then make the value of μ and D_{eff} reach the maximum. When D_θ becomes large, particles rotate faster, the effect of the external field

can be reduced, so μ and D_{eff} finally go to a constant. When the particles are without a magnetic field or subject to a rotating field, μ and D_{eff} increase with the increase of D_θ and remain nearly unchanged when γ is large. This is due to the competition between the external field and the rotational diffusion. From Figs. 10(c) and 10(d), we can find the mobility and the effective diffusion coefficient remain constant values for isotropic particles ($\Delta\Gamma = 0$), and are always larger than that of anisotropic particles. When $D_\theta \rightarrow 0$, the particle maintains its direction for a very long time and it is dominated by the translational diffusion. When $D_\theta \rightarrow \infty$, the particle rotates very fast and the influence of the particle anisotropy disappears, thus the mobility and the effective diffusion coefficient of anisotropic particles exhibit the same behaviors as that of isotropic particles finally.

By comparing with active particles, we can find that the mobility and the effective diffusion coefficient of passive particles have similar behaviors. In other words, the self-propelled velocity v_0 plays a key role in the difference between the transport and diffusive behavior. Additionally, the mobility and the effective diffusion coefficient of passive particles change a little when applying rotating magnetic fields of different frequencies. And the transport direction of passive particles can not be reversed by applying rotating magnetic fields.

Now we discuss the validity of the Einstein relation between diffusion and mobility in the case of passive particles. In equilibrium conditions, and in the linear regime, the Einstein relation predicts a proportionality between the diffusivity and the mobility, via the temperature [50],

$$D_x \equiv \mu k_B T. \quad (18)$$

We plot the ratio of the effective diffusion coefficient D_{eff} to the mobility μ of passive particles as a function of $\Delta\Gamma$, ω_c , ω_H , D_θ , f_0 , and $k_B T$ as shown in Figs. 11(a)-11(f), respectively. From Figs. 11(a)-11(e), it is found that the system is in the nonlinear regime, the ratio of D_{eff} to μ is changing in most cases while the ratio remains constant in the cases of $\Delta\Gamma = 0$ in Figs. 11(b)-11(d) and $\omega_c = 0$ in Fig. 11(c). From Fig. 11(f), we can find when f_0 and $k_B T$ is not small, the ratio of D_x to μ is not proportional to $k_B T$ and the system is in the nonlinear regime. However, the curves are near to be straight when f_0 and $k_B T$ is very small, the ratio of D_x to μ is nearly proportional to $k_B T$, the effect of f_0 and $k_B T$ is negligible, the system can be considered at equilibrium and satisfies the Einstein relation Eq. (18).

Finally, we discuss the possibility of realizing our model in experimental setups. Consider

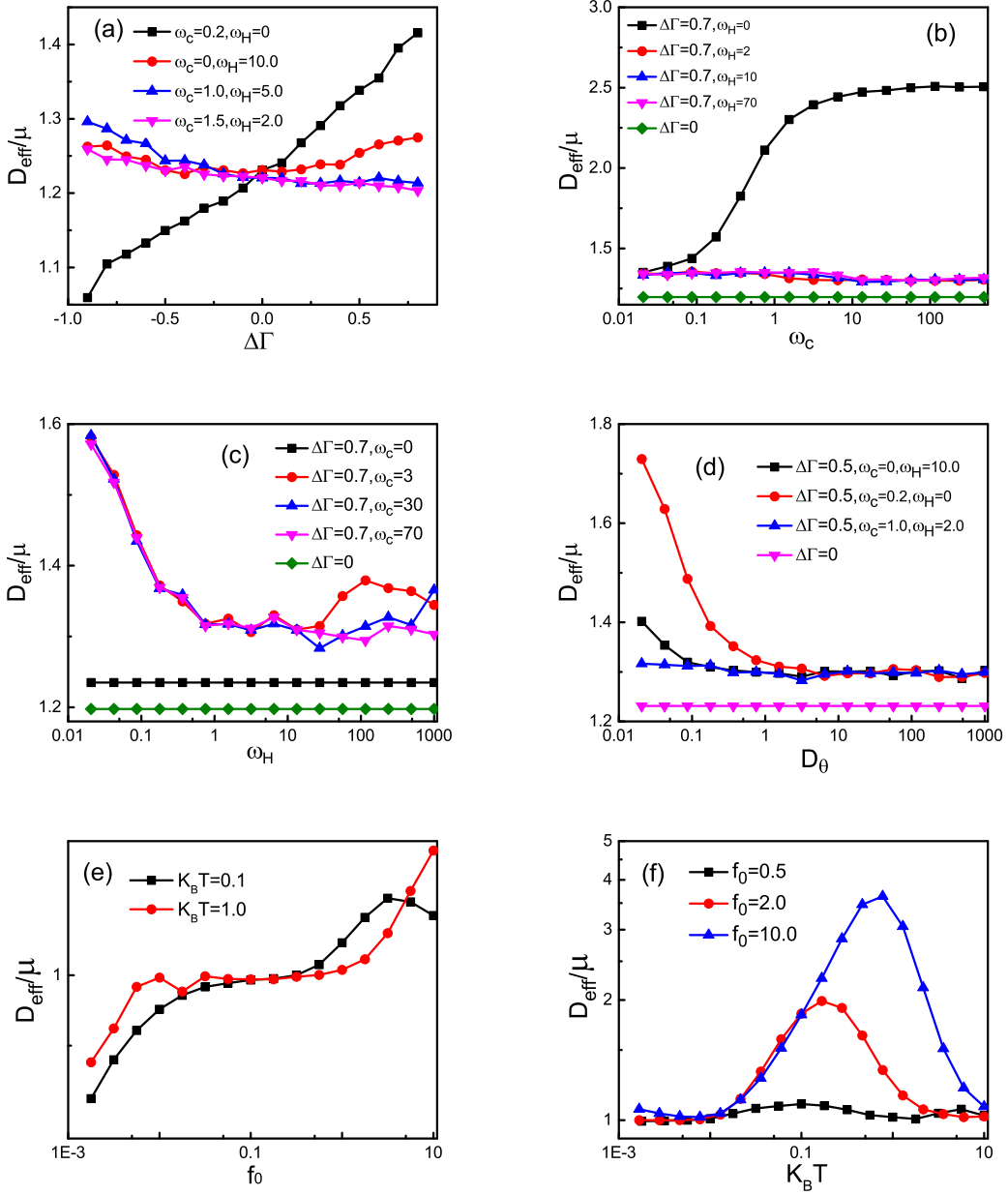


FIG. 11. The ratio of the effective diffusion coefficient D_{eff} to the mobility μ of passive particles (a) as a function of $\Delta\Gamma$ for different values of ω_c and ω_H at $k_B T = 1.0$; (b) as a function of ω_c for different values of $\Delta\Gamma$ and ω_H at $k_B T = 1.0$; (c) as a function of ω_H for different values of $\Delta\Gamma$ and ω_c at $k_B T = 1.0$; (d) as a function of D_θ for different values of $\Delta\Gamma$, ω_c and ω_H at $k_B T = 1.0$; (e) as a function of f_0 for different values of $k_B T$ at $\Delta\Gamma = 0$; (f) as a function of $k_B T$ for different values of f_0 at $\Delta\Gamma = 0$.

a system of paramagnetic ellipsoidal particles moving in a two-dimensional channel at room temperature. Paramagnetic ellipsoidal particles are obtained by adapting the method of Ref. [51] to commercially available magnetite-doped un-cross-linked polystyrene microspheres (Micromod GmbH, Germany). The channel is asymmetric and chosen to be corrugated structure. A rotating magnetic field in the particle plane is achieved by connecting two custom-made coils perpendicular to each other with the main axis along the (x, y) directions with a wave generator (TTi-TGA1244) feeding a power amplifier (IMG STA-800) [37, 38]. Due to the upper-lower asymmetry of the channel, paramagnetic ellipsoidal particles in a rotating magnetic field can produce the directed transport. To measure the motion of the paramagnetic ellipsoidal particles, we can image the particles by a high-speed camera, from which the average velocity and effective diffusion coefficient can be calculated. In the experimental setup, we can conveniently control the strength and frequency of rotating magnetic fields.

IV. CONCLUDING REMARKS

In this paper, we have numerically studied transport and diffusion of paramagnetic ellipsoidal particles under the action of a rotating magnetic field in a two-dimensional channel. It is found that paramagnetic ellipsoidal particles in a rotating magnetic field can be rectified in the upper-lower asymmetric channel. The transport and diffusion are sensitively influenced by the external magnetic field. For active particles, the rectification and the effective diffusion coefficient are much more different and complicated. The back-and-forth rotational motion facilitates the effective diffusion coefficient and reduces the rectification while the rotational motion synchronous with the magnetic field suppresses the effective diffusion coefficient and enhances the rectification. Applying different magnetic fields (static or rotating) or without magnetic field, the rectification and the effective diffusion coefficient of active particles with different shapes, self-propulsion velocities, and rotational diffusion rates exhibit different behaviors. It is due to the competition among the self-propelled velocity v_0 , the critical frequency ω_c , the magnetic frequency ω_H , the anisotropic parameter $\Delta\Gamma$, and the rotational diffusion rate D_θ . There exist optimized values of the parameters (the anisotropic degree, the amplitude and frequency of magnetic field, the self-propelled velocity, and the rotational diffusion rate) at which the average velocity and diffusion take

their maximal values. In addition, by applying rotating magnetic fields of suitable amplitude and frequency, three particle separation ways are presented: (1) shape separation: particles with $-0.4 \leq \Delta\Gamma \leq -0.9$ move to the left, whereas other particles move to the right; (2) self-propelled velocity separation: particles with $2.0 \leq v_0 \leq 5.0$ move to the left, whereas others move to the right; (3) rotational diffusion rate separation: particles with $D_\theta \leq 0.2$ move to the left, whereas others move to the right. Therefore, we can separate particles with different shapes, self-propelled speeds or rotational diffusion rates. For passive particles, the mobility and the effective diffusion coefficient have similar behaviors and change a little when applying rotating magnetic fields of different frequencies. The perfect sphere particle can facilitate the mobility and the effective diffusion coefficient, while the needlelike particle suppresses the mobility and the effective diffusion coefficient. The rotational motion synchronous with the magnetic field enhances the mobility and the effective diffusion coefficient, while the back-and-forth rotational motion reduces the mobility and the effective diffusion coefficient. There exists an optimal value of ω_H at which the mobility takes its maximal value. The position of the peak is nearly to $\omega_H \leq \omega_c$.

The results we have presented can characterize transport and diffusion of paramagnetic ellipsoidal particles in the previous experiment [37, 38]. It may open up the possibility of changing the frequency or strength of the applied magnetic field to separate particles, orient the particles along any direction at will during motion and control the particle diffusion in several applications, such as drug release and migration of contaminants in porous media. Furthermore, the anisotropic particles, like our paramagnetic ellipsoids, can be used as force sensors, microstirrers, active components in constrained geometries, microrheological probes or externally actuated micropellers [13]. Our analysis can be easily extended to more complex situations in the future, such as in the underdamped regime and consideration of particle interactions.

ACKNOWLEDGMENTS

This work was supported in part by the National Natural Science Foundation of China (Grants No. 11575064, No. 61762046 and No. 11704164), the Natural Science Foundation of Guangdong Province, China (Grants No. 2014A030313426 and No. 2017A030313029), the Natural Science Foundation of Jiangxi Province, China (Grants No. GJJ161580 and No.

GJJ160624), the Innovation Project of Graduate School of South China Normal University, and the Foreign Joint Training Program for PhD of South China Normal University.

- [1] X. Ao, P. K. Ghosh, Y. Li, G. Schmid, P. Hänggi, and F. Marchesoni, *Europhysics Letters* **109**, 10003 (2015).
- [2] P. S. Burada, P. Hänggi, F. Marchesoni, G. Schmid, and P. Talkner, *Chemphyschem* **10**, 45 (2009).
- [3] P. K. Ghosh, P. Hänggi, F. Marchesoni, and F. Nori, *Phys. Rev. E* **89**, 062115 (2014).
- [4] A. E. Antipov, A. V. Barzykin, A. M. Berezhkovskii, Y. A. Makhnovskii, V. Y. Zitserman, and S. M. Aldoshin, *Phys. Rev. E* **88**, 054101 (2013).
- [5] X. Wang, and G. Drazer, *Physics of Fluids* **21**, 102002 (2009).
- [6] Y. Li, P. K. Ghosh, F. Marchesoni, and B. Li, *Phys. Rev. E* **90**, 062301 (2014).
- [7] B. Q. Ai, and L. G. Liu, *Phys. Rev. E* **74**, 051114 (2006).
- [8] K. Lindenberg, J. M. Sancho, A. M. Lacasta, and I. M. Sokolov, *Physical Review Letters* **98**, 020602 (2007).
- [9] P. Reimann, and R. Eichhorn, *Phys. Rev. Lett.* **101**, 180601 (2008).
- [10] M. Khouri, A. M. Lacasta, J. M. Sancho, and K. Lindenberg, *Phys. Rev. Lett.* **106**, 090602 (2011).
- [11] P. Tierno, P. Reimann, T. H. Johansen, and F. Sagués, *Phys. Rev. Lett.* **105**, 230602 (2010).
- [12] R. Dreyfus, J. Baudry, M. L. Roper, M. Fermigier, H. A. Stone, and J. Bibette, *Nature* **437**, 862 (2005).
- [13] P. Tierno, *Physical chemistry chemical physics* **16**, 23515 (2014).
- [14] A. Cēbers and M. Ozols, *Phys. Rev. E* **73**, 021505 (2006).
- [15] Nicolas Waisbord, C. Lefèvre, Lydéric Bocquet, Christophe Ybert, and Cécile Cottin-Bizonne, *arXiv:1603.00490* (2016).
- [16] D. M. Fanlong Meng, and Ramin Golestanian, *arXiv:1710.08339* (2017).
- [17] T. Chen, X. B. Wang, and T. Yu, *Phys. Rev. E* **90**, 022101 (2014).
- [18] R. M. Erb, J. J. Martin, R. Soheilian, C. Pan, and J. R. Barber, *Advanced Functional Materials* **26**, 3859 (2016).
- [19] A. Snezhko, M. Belkin, I. S. Aranson, and W. K. Kwok, *Phys. Rev. Lett.* **102**, 118103 (2009).

[20] A. Snezhko, *Journal of Physics Condensed Matter An Institute of Physics Journal* **23**, 153101 (2011).

[21] A. Ghanbari, M. Bahrami, and M. R. H. Nobari, *Physical Review E* **83**, 046301 (2011).

[22] P. J. Vach, D. Walker, P. Fischer, P. Fratzl, and D. Faivre, *Journal of Physics D Applied Physics* **50** 11LT03 (2017).

[23] S. Babel, H. Löwen, and A. M. Menzel, *Europhysics Letters* **113**, 58003 (2016).

[24] F. Meshkati, and H. C. Fu, *Phys. Rev. E* **90**, 063006 (2014).

[25] I. S. M. Khalil, A. F. Tabak, A. Klingner, and M. Sitti, *Applied Physics Letters* **109**, 033701 (2016).

[26] J. E. Martin, *Phys. Rev. E* **79**, 011503 (2009).

[27] R. Marino, R. Eichhorn, and E. Aurell, *Phys. Rev. E* **93**, 012132 (2016).

[28] O. Güell, P. Tierno, and F. Sagués, *The European Physical Journal Special Topics* **187**, 15 (2010).

[29] Wai-TongLouis Fan, O. S. Pak, and M. Sandoval, *Physical Review E* **95**, 032605 (2017).

[30] D. Matsunaga, F. Meng, A. Zottl, R. Golestanian, and J. M. Yeomans, *Phys. Rev. Lett.* **119**, 198002 (2017).

[31] F. Liu, L. Jiang, H. M. Tan, A. Yadav, P. Biswas, J. R. van der Maarel, C. A. Nijhuis, and J. A. van Kan, *Biomicrofluidics* **10**, 064105 (2016).

[32] W. Gao, D. Kagan, O. S. Pak, C. Clawson, S. Campuzano, E. Chuluunerdene, E. Shipton, E. Fullerton, L. Zhang, and E. Lauga, *Small* **8**, 460 (2012).

[33] J. K. Hamilton, P. G. Petrov, C. P. Winlove, A. D. Gilbert, M. T. Bryan, and F. Y. Ogrin, *Sci. Rep.* **7**, 44142 (2017).

[34] T. Petit, L. Zhang, K. E. Peyer, B. E. Kratochvil, and B. J. Nelson, *Nano Letters* **12**, 156 (2012).

[35] P. Fischer, and A. Ghosh, *Nanoscale* **3**, 557 (2011).

[36] O. S. Pak, W. Gao, J. Wang, and E. Lauga, *Soft Matter* **7**, 8169 (2011).

[37] P. Tierno, J. Claret, F. Sagues, and A. Cébers, *Phys. Rev. E* **79**, 021501 (2009).

[38] P. Tierno, R. Albalat, and F. Sagues, *Small* **6**, 1749 (2010).

[39] B. ten Hagen, S. van Teeffelen, and H. Löwen, *J. Phys. Condens. Matter* **23**, 194119 (2011).

[40] R. Grima, and S. N. Yaliraki, *J. Chem. Phys.* **127**, 084511 (2007).

- [41] Y. Han, A. M. Alsayed, M. Nobili, J. Zhang, T. C. Lubensky, and A. G. Yodh, *Science* **314**, 626 (2006).
- [42] S. Denisov, P. Hänggi, and J. L. Mateos, *American Journal of Physics* **77**, 602 (2009).
- [43] O. Bénichou, P. Illien, G. Oshanin, A. Sarracino, and R. Voituriez, *Phys. Rev. Lett.* **113**, 268002 (2014)
- [44] O. Bénichou, P. Illien, G. Oshanin, A. Sarracino, and R. Voituriez, *Phys. Rev. E* **93**, 032128 (2016)
- [45] S. Leitmann and T. Franosch, *Phys. Rev. Lett.* **118**, 018001 (2017)
- [46] P. Illien, O. Bénichou, G. Oshanin, A. Sarracino, and R. Voituriez, *Phys. Rev. Lett.* **120**, 200606 (2018)
- [47] A. Sarracino, F. Cecconi, A. Puglisi, and A. Vulpiani, *Phys. Rev. Lett.* **117**, 174501 (2016)
- [48] F. Cecconi, A. Puglisi, A. Sarracino, and A. Vulpiani, *Eur. Phys. J. E* **40**, 81 (2017)
- [49] C. Reichhardt and C. J. O. Reichhardt, *J. Phys. : Condens. Matter* **30**, 015404 (2017)
- [50] A. Puglisi, A. Sarracino, and A. Vulpiani, *Physics Reports* **709-710**, 1-60 (2017)
- [51] J. A. Champion, Y. K. Katare, and S. Mitrugotri, *Proc. Natl. Acad. Sci. U.S.A.* **104**, 11901 (2007).